The Effect of Morphology on Solar Potential of High-Density Residential Area: A Case Study of Shanghai

Dan Zhu [1,*], Dexuan Song [1,*], Jie Shi [2], Jia Fang [1] and Yili Zhou [1]

[1] College of Architecture and Urban Planning, Tongji University, Shanghai 200092, China; 07fangjia@tongji.edu.cn (J.F.); zhouyili@tongji.edu.cn (Y.Z.)

[2] Chinesisch-Deutsche Hochschule für Angewandte Wissenschaften, Tongji University, Shanghai 200092, China; shijie@tongji.edu.cn

* Correspondence: 1zhudan_tju@tongji.edu.cn (D.Z.); dxsong@tongji.edu.cn (D.S.)

Abstract: This study explores the relationship between the morphology and solar potential of high-density areas in the subtropics high density city known as Shanghai. 1260 parametric scenarios were modeled and their solar irradiation potentials were simulated via a customized workflow. In addition to the five well-known morphological parameters, this study proposed two innovative morphological parameters SSU600 and SSU400, which captured the solar receiving properties of the building envelopes and could be easily calculated based on the meteorological data. For analytical purposes, the previously morphological parameters were considered as independent variables, whereas the new solar performance indicators SRU600 and SRU400 were both examined as dependent variables. The correlation analysis results suggested that the new morphological parameters displayed a strong linear correlation with the corresponding solar performance indicators, surpassing all the other morphological parameters. Two prediction models with respect to SRU600 and SRU400 were developed by multiple linear regressions using a stepwise method and their validity was verified by real residential cases. The findings provide key morphological parameters and rapid calculation tools for establishing solar energy friendly urban planning and design.

Keywords: solar energy potential; high-density residential area; morphological parameters; solar potential indicators; ladybug; multiple linear regressions

1. Introduction

1.1. Background

Currently, more than 50% of the world's population lives in cities, and this proportion is likely to grow up to 70% by 2050. Energy resource is a crucial necessity for urban development and the demand for energy is increasing with the development of urbanization. Cities are responsible for consuming roughly 80% of the energy production worldwide and it is expected that urban areas shall account for 74% of energy-related global greenhouse gases in 2030 [1]. Solar energy, as a kind of clean and abundant renewable energy source, has become the most applicable and suitable renewable energy source in cities with fast technological improvement, owing its related cost reductions and the public's growing acceptance [2]. Using buildings' surfaces to establish a distributed solar energy system can reduce land occupation and energy loss due to long-distance loosening, which is an effective way to meet cities' energy demand [3]. In accordance with *China's 13th Five-Year Plan for Energy Development*, the scale of solar power generation in China will exceed 100 million kilowatts by 2020, and more than half of them will be generated by a distributed photovoltaic power generation system [4]. Large scale application of

photovoltaic on roofs and facades of urban buildings is the principal way of constructing distributed photovoltaic system [5]. *Regulations on Energy Conservation of Buildings of Shanghai* demonstrate that the solar thermal (ST) system is highly recommended for all new residential buildings [6].

In addition to the solar module and system technologies and intensity of isolation, the availability of suitable spaces for solar system installation is also significant factor for solar harvesting and which is related to urban morphology. High-density cities face more challenges in regard to solar receiving than low-density urban areas. There are substantial mutual shading and self-shading for buildings in high-density areas and not all building envelopes are suitable to deploy solar systems such as PV panels or solar thermal modules. It has been revealed by previous study that given the same urban context and built density, the environmental performance including solar potential of different schemes may vary significantly [7]. Therefore, it is important to investigate the relationship between solar potential and urban morphology from the perspective of urban planning and design.

1.2. Urban Morphology and Solar Energy Potential

Based on the goals of maximizing solar irradiation receiving of the building facade, a new residential design pattern "Residential Solar Block" (RSB) at the north latitude 48° was proposed by Okeil [8]. By comparing with the linear form and block form, it was proved that the RSB layout can maximize the use of solar energy on the exterior envelope of the building, and at the same time the RSB pattern combined the functional, special, and visual advantages. Leung [9] took the tropic city Singapore and Dubai as examples to explore the relationship between the amount of solar irradiation received by the facades of high-density residential buildings and the building form. The results showed that only when the building density reached a certain level and the building was south-facing, the building form would have a significant effect on the amount of solar irradiation receiving by building facade. Kanters and Wall [10,11] of Lund University in Sweden evaluated the influence of typical design-related morphological factors (layout, building density, building orientation, and roof form) on the solar irradiation potential. The results showed that building density had significant effect (up to 50%) on solar energy production, while the influence of building orientation was not obvious. Another achievement of the research was the development of a website named solar planning [12]. Users can choose a specific combination of building design factors according to the situation. After input or choose the design parameters, the website would generate a solar evaluation report online for relevant personnel to make preliminary comparisons and judgments. Similarly, Dapeng Li et al. [13] investigated the effects of three major design parameters, such as aspect ratio, azimuth, and site coverage on solar potential (photovoltaic and solar thermal), and the findings showed that increasing building aspect and site coverage tended raise solar potential. In contrast, Mohajeri at al. [14] found that with increasing compactness, the potential of BiPV, STC and passive solar heating decreased significantly. In Canada, Caroline Hachem et al. [15] took two-story single-family house as research objects and studied the impact of different building orientation, building form (rectangular, L-shaped, Y-shaped, etc.) and building combination (single-family, row) on the potential of solar photovoltaic power generation. The result suggested that, compared with the reference layout, certain shape-site configurations could achieve a significant electricity generation increase (up to 33%).

The study of Peronato [16] took a typical urban renewal project as an example and the results showed that the block width had a stronger correlation with daylight compared with building height or setback distance of the building. Christina Chatzipoulka [17] explored the relationship between sky view factor and global irradiation for 30 orientations of three European climates (Athens, London, and Helsinki) and three periods (year, January, and July). A strong linear relationship was revealed in all 30 orientations and at all three locations, which was in line with the findings by the other researchers [18,19]. Cheng [20] adopted a parametric approach to explore the best urban layout from the perspective of solar energy utilization taking São Paulo, Brazil an example. The study compared the solar energy of homogeneous layout, randomness in horizontal layout and randomness in vertical layout. The results showed that randomness in vertical layout was most conducive to the incidence of

sunlight. Also, the results suggested that higher buildings and less site coverage were preferable to lower buildings and higher site coverage.

Previous researchers carried out research on the correlation between urban morphology and solar potential from different perspectives. Most of them are limited to a few typical patterns with obvious regularity, and the conclusions have no malleability. Some studies take into account of the quantitative control parameters of residential morphology, while the number of samples is not large enough, so it is hard to make a comprehensive description of urban residential morphology. Also, there is a lack of targeted and explanatory morphological parameters for the potential of solar irradiation.

This study, taking Shanghai as an example, aims to examine the quantitative relationship between the morphology of high-density residential area and solar energy potential systematically through simulation-based method and propose the key morphological parameters and prediction tools regarding to solar energy potential.

2. Methods

2.1. Background

2.1.1. High-Density Residential Area in Shanghai

Shanghai (31.2° N, 121.5° E) lies on the east coast of China and is part of the alluvial plain of the Yangtze River Delta with an average altitude of 2.19 m and it is equally situated in the subtropical zone with the monsoon climate. It is one of China's largest and densest cities. Shanghai's residential area design and construction are highly representative and typical.

With the rapid urbanization process, standardized and replicable residential layouts and designs were adopted by real estate developers in pursuit of economic benefits, which led to the convergence of texture in residential areas. Through the statistical analysis of Shanghai's 365 residential cases, it is clear that linear layouts were adopted as a configuration prototype by about 88% of the residential cases. On the basis of the prototype, east–west and south–north staggered were also common layouts to capture more daylight and better landscape views. A typical residential model was extracted as illustrated in Figure 1 [21].
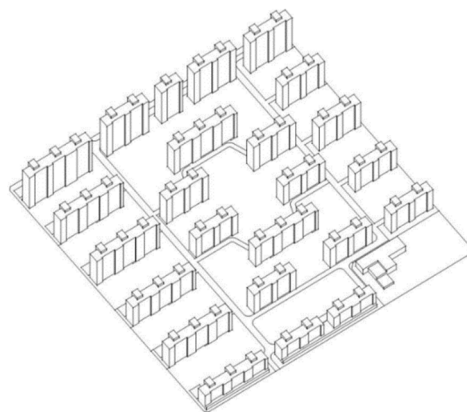
Figure 1. Typical residential model of Shanghai.

2.1.2. Solar Energy Resource in Shanghai

In Shanghai, the annual cumulative global horizontal solar irradiation is 1204.25 kWh/m^2/y and the annual cumulative solar irradiation of each orientation's vertical facade is presented in Table 1 and Figure 2. The true north refers to 0 degrees, moving in a clockwise direction from 0–360 degrees. Shanghai sits on the brink of the East China Sea and it has a heavier cloud cover in the morning than the afternoon. Therefore, it can be observed from Figure 2 that south by west orientation is more favorable for solar reception compared with the south by east. More specially, the orientation range of

facades receiving annual solar irradiation above 400 kWh/m^2/y is 70–315°. As to those with receivable annual solar irradiation higher than 600 kWh/m^2/y, the orientation range is 140–270°. The maximum receivable annual irradiation of the facades is 712.8 kWh/m^2, with an orientation of 220°. Thence, there are significant discrepancies in the amount of annual solar irradiation received by the same building's facades, mostly due to different orientations and inclination angles.

Table 1. Annual solar irradiation received by unit vertical facade area of each orientation in Shanghai (unit: kWh/m^2/y).

Orientation [1.]	Annual Solar Irradiation	Orientation	Annual Solar Irradiation	Orientation	Annual Solar Irradiation
5°	255.50	125°	575.77	245°	686.66
10°	257.44	130°	586.69	250°	675.54
15°	260.67	135°	595.44	255°	661.21
20°	269.06	140°	606.25	260°	647.36
25°	278.53	145°	615.12	265°	630.06
30°	285.88	150°	619.31	270°	607.96
35°	301.86	155°	631.57	275°	591.53
40°	315.54	160°	639.03	280°	570.59
45°	328.97	165°	644.40	285°	546.81
50°	345.27	170°	652.19	290°	524.18
55°	361.07	175°	658.58	295°	499.52
60°	376.44	180°	663.87	300°	473.16
65°	394.80	185°	673.43	305°	449.71
70°	412.16	190°	682.12	310°	425.39
75°	428.32	195°	682.12	315°	399.12
80°	446.73	200°	697.52	320°	378.41
85°	463.22	205°	703.99	325°	356.49
90°	476.18	210°	705.10	330°	331.86
95°	495.80	215°	711.66	335°	317.50
100°	511.66	220°	712.80	340°	300.72
105°	525.11	225°	710.65	345°	284.41
110°	539.88	230°	708.48	350°	273.28
115°	552.51	235°	703.04	355°	263.62
120°	563.03	240°	694.57	360°	255.87

[1] True north is 0 degrees and go clockwise are 0~360 degrees in turn.
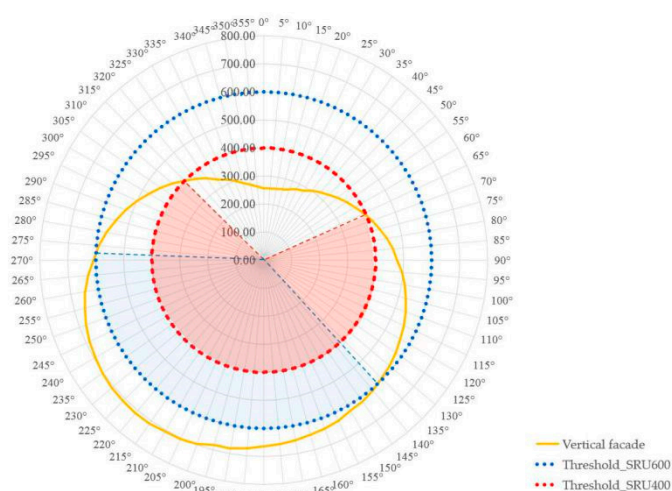
Figure 2. Annual solar irradiation received by unit vertical facade area of each orientation in Shanghai (unit: kWh/m^2/y).

2.2. Parametric Models Building

A parametric approach was implemented in this study in order to focus the research on the relationship between the morphology and solar potential while ruling out the interference of non-design factors. Based on the statistics of typical residential areas in Shanghai, combined with those of relevant research articles [22–27] and the design code [28], the morphological characteristics and parameters of typical residential areas were extracted and summarized, and were then used as the standard for establishing the experimental parametric models. This method allows for quick set up of a vast number of morphological scenarios to ensure the morphological possibility coverage of the typical residential areas; and the morphological variables can be adjusted as needed to ensure the comparability between the scenarios.

The experimental parametric scenarios were established according to the following criteria (see Figure 3):

(a).　Site and surroundings

According to the road network density and the statistical data of residential area scales in Shanghai [28], the site size was set as a 300 × 300 m square-shape with a 20 m width road around, with site areas of 90,000 square meters. The distance between the building setback boundary line and the road was 15 m. The layout and building's height of the surrounding eight plots were the same as the experimental plots.

(b).　Single building form

It was set as a slab type building with a width of 30 m and a depth of 15 m.

(c).　Orientation

The orientations of the square-shape site varied from 135° to 225° with 15° increments, so that the orientation values were 135°, 150°, 165°, 180°, 195°, 210°, 225°. (due north was set to 0°).

(d).　Layout

Linear (with both row alignment and column alignment); east–west staggered (just with row alignment) and south–north staggered (just with column alignment).

(e).　Building height

According to the data of the most common building heights, the building heights here were set as 12, 18, 33, 54, 78, and 99 m.

(f).　Building density

In this study, building density was represented by the number of rows and columns. The number of rows was determined as 3, 4, 5, 6, 7, and 8, and the number of columns was configured as 4, 5, and 6.

Modeling according to the above-mentioned parameters' combination, a total of $3 \times 7 \times 6 \times 6 \times 3 \times$ = 2268 scenarios were generated. Removing the scenarios that do not meet the design code in Shanghai (there must be a valid sunshine duration of no less than one hour in the winter solstice for at least one bedroom of the first-floor apartment), and a total of 1260 experimental scenarios were developed.
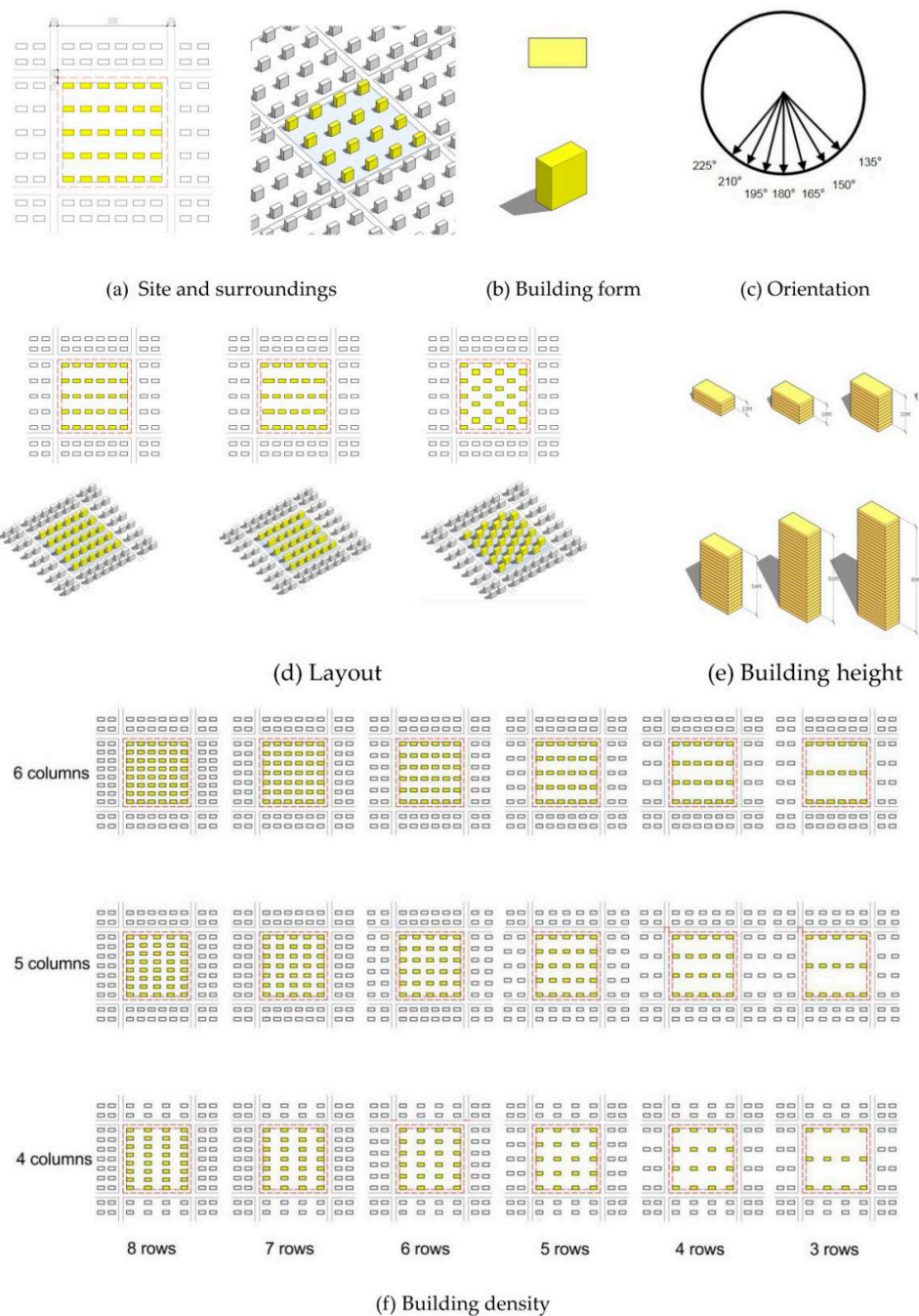
(a) Site and surroundings　　　(b) Building form　　　(c) Orientation

(d) Layout　　　　　　　　　　　　(e) Building height

6 columns

5 columns

4 columns

8 rows　　　7 rows　　　6 rows　　　5 rows　　　4 rows　　　3 rows

(f) Building density

Figure 3. Establishing criteria for all parametric models.

2.3. Solar Performance Indicators

Compagnon proposed thresholds of solar potential based on the annual cumulative solar irradiation received by unit building surface [29]. In this study, whilst taking comprehensive consideration of the existing technological level and economic benefits, the thresholds were set to 600 kWh/m^2/y and 400 kWh/m^2/y. Figure 4 illustrates that the qualified surface areas for two thresholds of a residential area in Shanghai's city context and irradiation conditions. It can be seen that the qualified surface areas were different according to different thresholds due to the mutual shading of the buildings. Based on these thresholds, two solar potential indicators were calculated, quantifying the annual solar irradiation received by building surface relative to gross floor area which named as SR_{U600} and SR_{U400} respectively. The indicator was calculated for the qualified building surface areas

with annual cumulative irradiation exceeding 600 kWh/m^2 or 400 kWh/m^2 only. SR$_{U600}$ and SR$_{U400}$ were obtained by summing up the solar irradiation of all the selected surfaces and then dividing the result by the GFA.
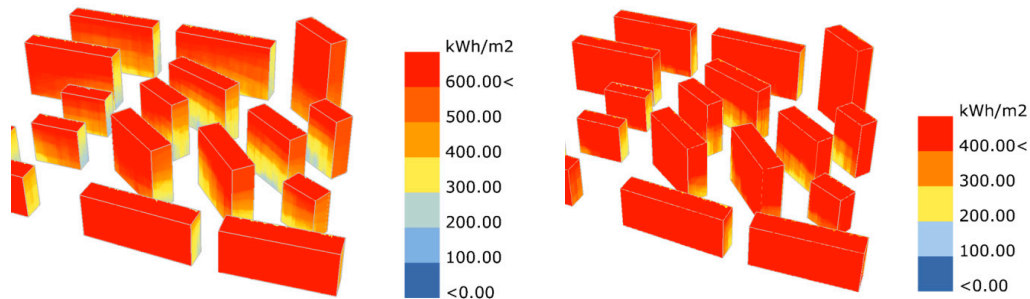
Figure 4. Qualified surface areas for 600 kWh/m^2/y (**left**) and 400 kWh/m^2/y (**right**) of a residential area in Shanghai.

2.4. Morphological Parameters

In order to present a more comprehensive description of the residential area's morphological characteristics, whilst taking the literature reviews on urban indices as reference, five conventional morphological parameters have been selected and two new parameters were defined for all the 1260 parametric models.

1. Gross floor area (GFA).
2. Floor area ratio (FAR), FAR = GFA/site area.
3. Building density (BD), BD = building footprint area/site area.
4. Building height (BH), BH = GFA/building footprint area.
5. Open space ratio (OSR), OSR = unbuilt area/GFA [30].
6. SS$_{U600}$.
7. SS$_{U400}$.

Aiming at capturing the solar receiving performance of the building envelope surfaces, two additional parameters were defined and examined which quantify the weighted surface area relative to the GFA. The new morphological parameters are denoted as SS$_{U600}$ and SS$_{U400}$ respectively.

The following takes SS$_{U600}$ in Shanghai as an example to explain the calculation method of the new parameters.

(a). The first step was to select building surfaces with annual solar irradiation beyond 600 kWh/m^2/y and calculate their surface area one by one. The selected surfaces were recorded as F$_1$, F$_2$ ... F$_n$, and their surface area were recorded as FA$_1$, FA$_2$ ... FA$_n$;

(b). The second step was to obtain the solar irradiation of each selected surface by meteorological database which were recorded as S$_1$, S$_2$ ... S$_n$. Each surface's weighting coefficient was the ratio of S$_1$, S$_2$ ... S$_n$ to 600, denoted as R$_1$, R$_2$ ... R$_n$. Taking the south facade as an example, it can be derived from Table 1 that the annual irradiation received by the south facade was 663.87 kWh/m^2/y, implying that the south facade's weighting coefficient was determined as 667.83/600 = 1.11.

(c). Finally, it was to multiply the area of each selected surfaces with the corresponding weighting coefficients and sum them. Then the value of sum was divided by the GFA.

$$SS_{U600} = \frac{FA_1 * R_1 + FA_2 * R_2 + \ldots + FA_n * R_n}{GFA} \tag{1}$$

Table 2 displays the comparisons of the surface area per unit floor area (SS$_U$), SS$_{U600}$ and SS$_{U400}$ of a single building with different orientations (width = 30 m, length = 15 m, and height = 33 m).

Different building envelopes were selected due to different orientations and thresholds. As shown in Table 2, selected facades were marked with red lines in plans while roofs were selected for all scenarios. Also, it can be seen that the SS_U at different building orientations are the same, whereas the SS_{U600} and SS_{U400} are different from each other. The lowest and highest orientations of the SS_{U600} value were 135° and 165° respectively, which were 68.4% higher than those of the former. Meanwhile, regarding the SS_{U400} value, the lowest and highest orientations were 225° and 210° respectively, which was 30.5% higher than those of the former.

Table 2. SS_U, SS_{U600}, and SS_{U400} of a single building with different orientations.

	225°	210°	195°	180°	165°	150°	135°
Schematic Diagram							
SS_U [1]							
	0.691	0.691	0.691	0.691	0.691	0.691	0.691
SS_{U600}							
	0.419	0.417	0.410	0.505	**0.507**	0.506	0.301
SS_{U400}							
	0.678	**0.885**	0.883	0.877	0.868	0.757	0.749

[1] SS_U is defined as the surface area per unit floor area.

2.5. Workflow

The workflow of this research was composed of three parts of modeling, simulation as well as data processing and analysis (see Figure 5). Firstly, the software Rhinoceros3D and the parametric modeling plug-in Grasshopper were used for modeling. Next, the solar irradiation for all scenarios were simulated by radiance-based simulation plug-in Ladybug. The data processing and analysis software were Excel and SPSS, and the output was recorded as visual simulation images and data analysis graphs. The meteorological data used for solar irradiation simulation was derived from the Energy Plus weather database [31].
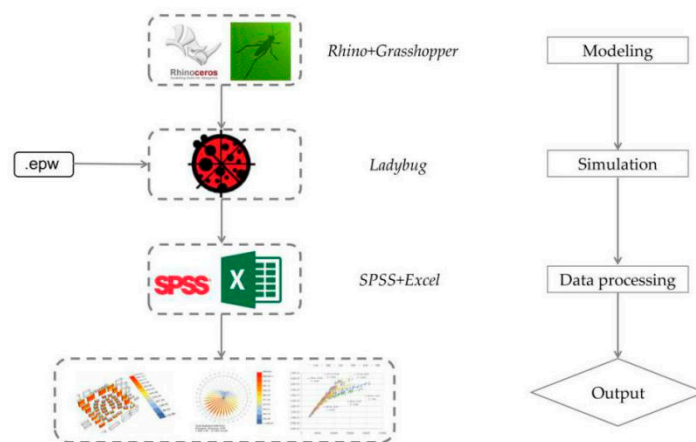
Figure 5. Workflow developed in this research.

The typical parameters of Ladybug were configured as portrayed in Table 3.

**Table 3.** Parameters setting for solar energy simulation via ladybug.

Parameter	Setting
Computing grid	1×1 m
Weather data	China standard weather data (CSWD)
Start date	1 January
End data	31 December
Hour range	00:00–24:00
Computing interval	1 h
Solar radiation model	GenCumulative Sky
Location	Shanghai

Firstly, all of the 1260 scenarios were modeled in accordance with the rules set out above by Rhino and Grasshopper. Windows and equipment installation were considered to cover 30% of the facade and roof area. The second step was to simulate the annual irradiation on the building envelope surfaces (both facades and roofs) via Ladybug, which were divided into 1×1 m grids. The simulation results were exported as a list of all mesh surfaces with their respective coordinate information and annual irradiation values. The mesh surfaces were then divided into three categories according based on the simulation results: (1) less than 400 kWh/m^2/y, (2) no more than 600 kWh/m^2/y, and (3) no more than 400 kWh/m^2/y. For categories (2) and (3), each group's solar irradiation was summed up and the result was divided by the gross floor area (GFA) gives the respective SRU600 and SRU400 values.

3. Results

3.1. Correlation Analysis

Figure 6 outlines the scatter plots of the linear regress analysis between the solar indicator SR_{U600} and morphological parameters of the 1260 scenarios. From the regression analysis results, it can be stipulated that the new morphological parameter SS_{U600} was the most significant factor with respect to SR_{U600} (R2 = 0.874), followed by building height (R2 = 0.741), FAR (R2 = 0.723), and GFA (R2 = 0.723). OSR (R2 = 0.596) had lesser extents impact, while the least relevant factor was building density (R2 = 0.104). It should be noted that the influence of the FAR and GFA were identical, due to the existing mathematical correlation between them in terms of the fixed site area.
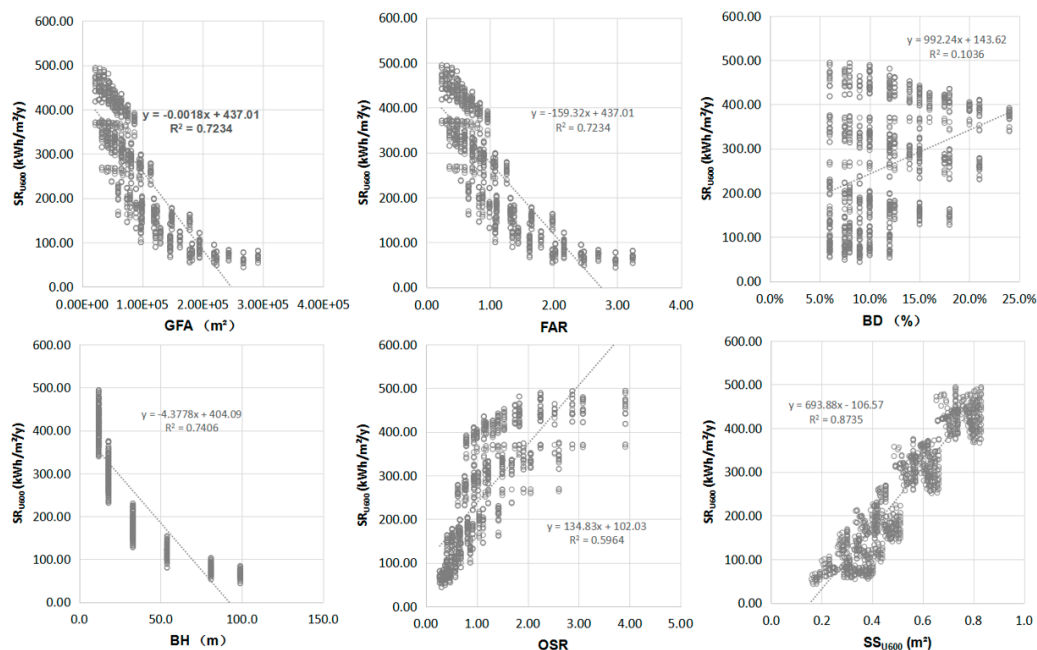
Figure 6. Scatter plots and results of linear regression analysis for the SR_{U600} and morphological parameter.

Moreover, Figure 7 depicts the linear regress analysis results between the solar indicator SR_{U400} and morphological parameters. Similar with the results of SR_{U600}, the new indicator SR_{U400} was the most significant factor (R2 = 0.933). Building height (R2 = 0.804), FAR (R2 = 0.769), GFA (R2 = 0.769), and OSR (R2 = 0.554) were also strongly correlated. Building density (R2 = 0.139) exhibited the weakest correlation.
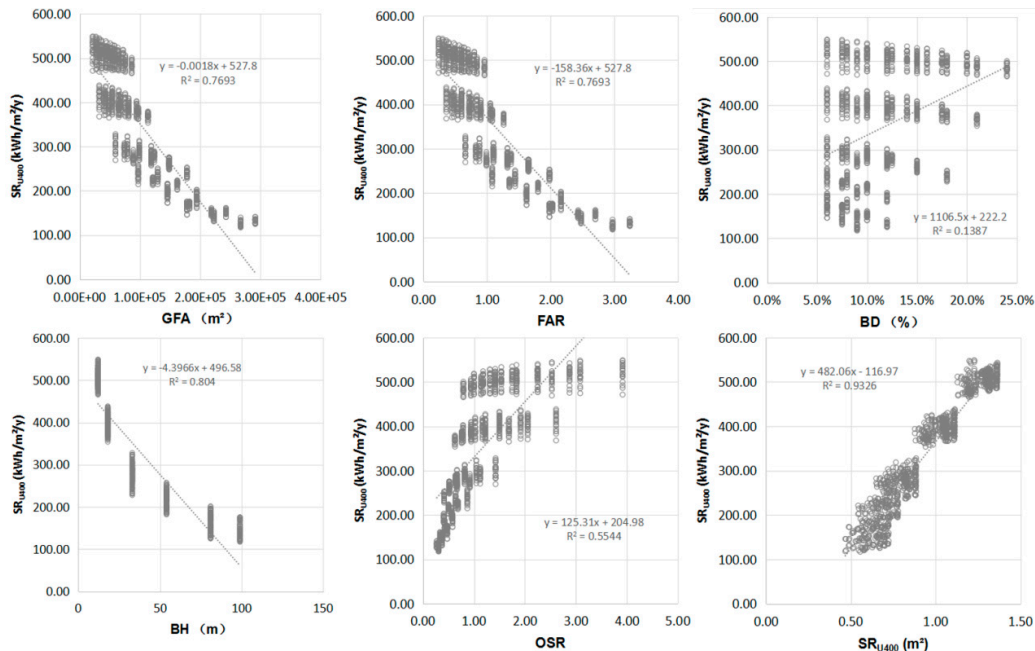
Figure 7. Scatter plots and results of linear regression analysis for the SRU400 and morphological parameter.

3.2. Prediction Model

The correlation analysis above describes a one-to-one correlation ship between the morphological parameters and the solar potential indicators. In order to build a more thorough quantitative description between them, it was assumed that SR_{U600} and SR_{U400} could be predicted as a linear function of their corresponding morphological parameters. The SPSS software was used to perform a multiple linear regression analysis via the stepwise regression method. In the stepwise expression, the principle of variable selection is as follows: Under the linear condition, the variables were contained in a combination of variables which explains the fact that more dependent variable discrepancy will be selected. Taking SR_{U600} as a dependent variable, there were 4 indicators including SS_{U600}, FAR, OSR, and BH entering the regression model after four iterations of the stepwise regressions (Table 4). Their *p* value of significance was 0.000 ($p < 0.001$) which indicated that the data was statistically significant. Based on the multiple regression results, the linear regression equation can be established as

$$SR_{U600} = 36.833 + 435.018*SS_{U600} - 17.884 \times FAR + 38.078*OSR - 0.876BH \qquad (2)$$

In the same way, taking SR_{U400} as the dependent variable, there were 4 indicators including SS_{U400}, FAR, BH, and OSR joining the regression model after four iterations of the stepwise method (Table 5).

$$SR_{U400} = 83.178 + 326.466*SS_{U400} - 36.931 \times FAR - 0.614 \times BH + 12.160*OSR \qquad (3)$$

The rightmost column of Tables 4 and 5 highlighted that the collinear statistical values VIF (variance inflation factor) of the respective variables were all less than 10, suggesting that there is no significant collinearity of the respective variables and the regression Equations (2) and (3) are workable. The validity of the regression equations above will be verified further below.

Table 4. Multiple linear regression models for SR_{U600} of 1260 scenarios in Shanghai.

	Model	Beta	StdBeta	*p*-Value	Beta (95% CI)		Collinearity Statistics	
					Lower Limit	Upper Limit	Tolerance	VIF
1	Constant value	−102.718		0.000	−110.784	−94.652		
	SS_{U600}	692.975	0.934	0.000	678.348	707.602	1.000	1.000
2	Constant value	71.894		0.000	59.475	84.313		
	SS_{U600}	499.752	0.674	0.000	483.505	515.999	0.453	2.206
	FAR	−65.931	−0.352	0.000	−70.029	−61.832	0.453	2.206
3	Constant value	20.868		0.001	8.021	33.715		
	SS_{U600}	480.799	0.648	0.000	465.856	495.741	0.443	2.258
	FAR	−43.627	−0.233	0.000	−48.217	−39.038	0.299	3.348
	OSR	31.075	0.178	0.000	27.340	34.810	0.391	2.556
4	Constant value	36.833		0.000	24.104	49.562		
	SS_{U600}	435.018	0.586	0.000	418.164	451.872	0.322	3.107
	FAR	−17.884	−0.096	0.000	−24.519	−11.249	0.132	7.566
	OSR	38.078	0.218	0.000	34.243	41.914	0.343	2.916
	BH	−0.876	−0.172	0.000	−1.044	−0.707	0.151	6.613

Table 5. Multiple linear regression models for SR_{U400} of 1260 scenarios in Shanghai.

	Model	Beta	StdBeta	*p*-Value	Beta (95% CI)		Collinearity Statistics	
					Lower Limit	Upper Limit	Tolerance	VIF
1	Constant value	−114.117		0.000	−121.317	−106.918		
	SS_{U400}	481.561	0.965	0.000	474.351	488.771	1.000	1.000
2	Constant value	72.695		0.000	63.529	81.861		
	SS_{U400}	356.102	0.714	0.000	349.124	363.080	0.403	2.481
	FAR	−58.717	−0.325	0.000	−61.240	−56.194	0.403	2.481
3	Constant value	91.165		0.000	80.997	101.333		
	SS_{U400}	340.612	0.683	0.000	332.690	348.535	0.299	3.341
	FAR	−49.860	−0.276	0.000	−53.233	−46.487	0.216	4.631
	BH	−0.406	−0.083	0.000	−0.511	−0.300	0.164	6.110
4	Constant value	83.178		0.000	73.240	93.116		
	SS_{U400}	326.466	0.654	0.000	318.313	334.618	0.263	3.803
	FAR	−36.931	−0.205	0.000	−41.094	−32.769	0.132	7.581
	BH	−0.614	−0.125	0.000	−0.724	−0.504	0.140	7.148
	OSR	12.160	0.072	0.000	9.718	14.602	0.332	3.010

4. Case Verification

The main purpose of this section is to verify the validity of the results of correlation analysis and prediction models using real cases in Shanghai.

4.1. Case Study 1

The results obtained in Section 3.1 proved that there was a strong correlation between the new morphological parameters s SS_{U600}/SS_{U400} and the solar indicator SR_{U600}/SR_{U600}. To verify these correlations, a residential case of Shanghai was picked as the benchmark for a comparative study. As presented in Table 6, the current configuration was a linear layout with slab buildings facing about 30 degrees south by west.

The objective of the schemes put forward so far was to boost the solar energy potential by increasing SS_{U600}/SS_{U400}. Each scheme's optimization strategies were designed as follows (Table 6):

Scheme A: The orientation of the buildings was fixed with lower building heights and increasing the number of buildings so as to raise the total surface area of roofs.

Scheme B: The orientation of the buildings was altered from west by south to due south with the fixed footprint area and building height.

Scheme C: The depth of the building was shortened and the width of the surface was widened to ensure that the footprint areas remain fixed.

Simplified building models were developed while maintaining the same level of abstraction about building forms. The solar energy potential comparisons of the existing and proposed schemes were conducted using the same workflow.

Table 6. Schematic master plans and morphology parameters statistics of existing and proposed schemes.
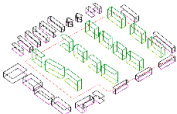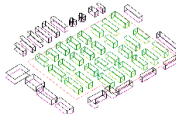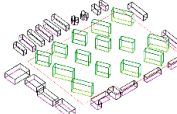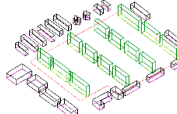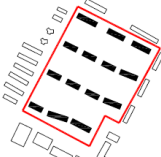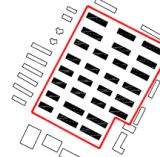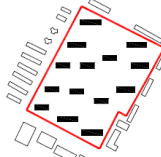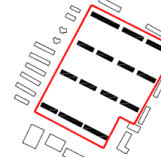
	Existing Design	Scheme A	Scheme B	Scheme C
Aerial view				
Schematic Master Plan				
GFA	118,800	118,800	118,800	118,800
FAR	1.39	1.39	1.39	1.39
BD	11.6%	23.2%	11.6%	11.6%
BH	36.0	18.0	36.0	36.0
SS_{U600}	0.40	0.57	0.46	0.46
SS_{U400}	0.77	1.02	0.76	0.83

Figure 8 shows the comparison between the existing scheme and proposed schemes with respect to the SS_{U600} and SR_{U400}. In general, the result showed that the variation trends of SR_{U600} was consistent with that of SS_{U600}. It can be stated that compared with the existing design, the SS_{U600} of the three proposed designs increased 42.5%, 14.6%, and 15.9% respectively, and also induced an overall increase of 38.0%, 10.2%, and 12.1% of the SR_{U600}, respectively. The simulation results confirmed that the largest augmentation in SR_{U600} was that of scheme A for the roof area was doubled with the facade area fixed. As visible in Table 2, due to the fact that the south was more advantageous than the south by west orientation regarding SS_{U600}, so the SR_{U600} value of scheme B was also increased to a certain extent. Concerning scheme C, the area of the facade facing south to west was enlarged to increase the SS_{U600} value which brought about a raise of the SR_{U600}.

Figure 8. Comparison of SS_{U600} and SR_{U600} between existing scheme and proposed schemes.

Figure 9 illustrates *t* the comparison between the existing and proposed schemes in terms of SS_{U400} and SR_{U40}. Again, in general, the change of SR_{U400} was close accord with that of SS_{U400}. It can be seen that, similar with Figure 8, the biggest percentage jump of SS_{U400} and SR_{U400} was in scheme A, and the growth rates were 32.5% and 33.1% respectively. The second was scheme C with growing rates of 7.5%

and 5%. It is worth mentioning that there was a slight decrease in the SS_{U400} and SR_{U400} for scheme B (0.9% and 3.1%, respectively). This decline could be accounted for by the fact that compared with the south by west orientation, due south was an unfavorable orientation regarding SS_{U400} (See Table 2).
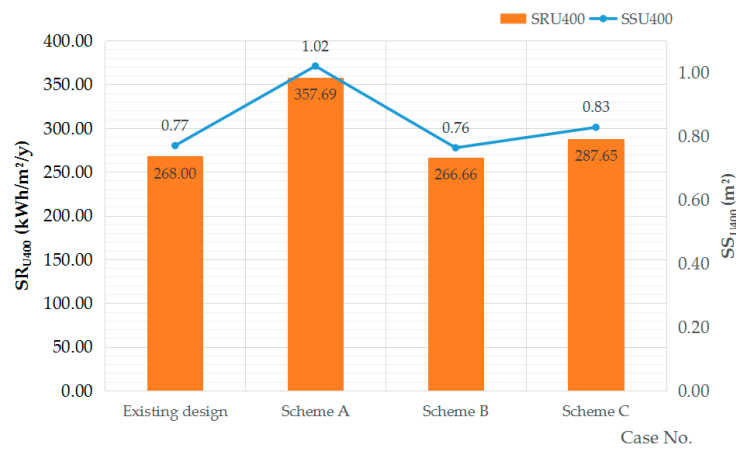

Figure 9. Comparison of SS_{U400} and SR_{U400} between existing scheme and proposed schemes.
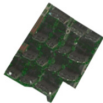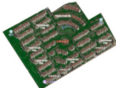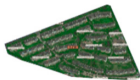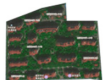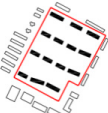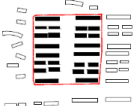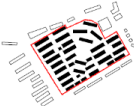
4.2. Case Study 2

In a real city, affected by many factors such as the road network distribution, shape of the plot, design code and economic benefits, it is difficult for the residential morphology to be in complete agreement with the parameter scenarios. The main purpose of this section is to verify the solar energy potential prediction model based on the parameter models set forth earlier in this study through comparison between the simulation values and prediction values of the actual residential cases. The criteria for case selection were as follows:

1. The area of the plot was close to 90,000 sq.m;
2. The plot was dominated by slab and vertical homogeneous buildings;
3. The range of the morphological parameters of all the cases should be within the boundary conditions of the parametric scenarios.

Five real residential area cases were selected and Table 7 shows the schematic master plans and morphology parameters statistics of all five cases.

Table 7. Schematic master plans and morphology parameters statistics of five cases.

	Case 01	Case 02	Case 03	Case 04	Case 05
Aerial map					
Schematic Master Plan					
GFA	118,800	129,528	149,202	114,492	123,836
FAR	1.39	1.64	1.72	1.40	1.46
BD	11.6%	27.3%	28.7%	23.4%	18.3%
BH	36.0	18.0	18.0	18.0	24.0
OSR	0.64	0.45	0.41	0.55	0.44
SS_{U600}	0.40	0.61	0.62	0.62	0.48
SS_{U400}	0.77	0.96	0.95	1.00	0.81

On the one hand, the five cases were modeled with the same level of abstraction about building form, and the simulation values of SR_{U600} and SR_{U400} were obtained by simulation via the workflow

introduced above. On the other hand, the morphological parameters of the five cases were treated as independent variables into the Equations (2) and (3) to get the calculated values and prediction ranges of SR_{U600} and SR_{U400} (the confidence interval was set to 95%). Figures 10 and 11 highlight the comparison between the simulation values and predicted values. The red lines mark the simulation values and the box-plots delineate the prediction ranges. If the box-plot is above the red line mark, it indicates that the predicted value is higher than the simulation value; if the box-plot is below the red line mark, it suggests that the predicted value is lower than the simulation value; meanwhile, if the box-plot contains the red line, the prediction is considered accurate. It is quite obvious that the prediction values of SR_{U600} and SR_{U400} in four of the five cases were precise, whereas the predicted values of case 04 were inconsistent with the simulation values. The percentages of deviation value of SR_{U600} and SR_{U400} for case 4 were 3% and 6% respectively.
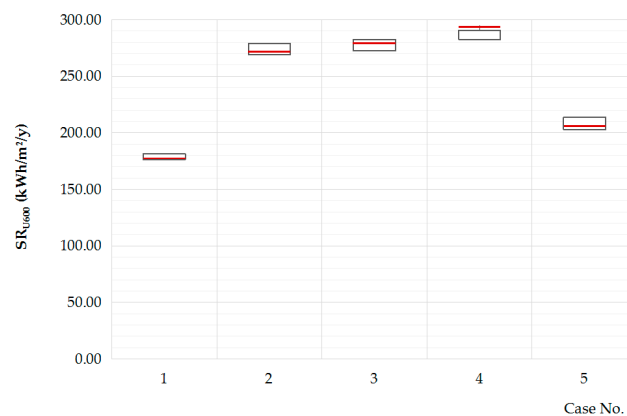

Figure 10. Comparison between the simulation and predicted values of SR_{U600}.
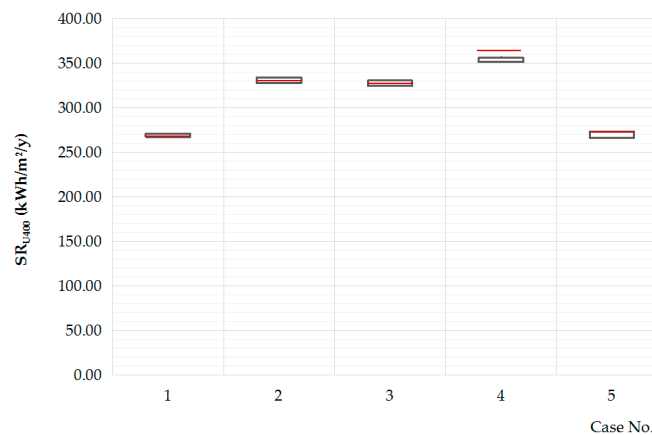

Figure 11. Comparison between the simulation and predicted values of SR_{U400}.

5. Discussion

5.1. Correlation between the New Morphological Parameters and Solar Potential

In order to express the solar receiving performance of building surface, the new aforementioned indicators SS_{U600} and SS_{U400} were put forward, which indirectly encompass information such as the geographic location, weather data and building orientation. The weighting coefficient acted as 'leverage', which can eliminate or weaken the interference of surfaces absorbing less solar irradiation, while expanding or strengthening the influence of the surface receiving more solar irradiation.

The results of the correlation analysis also prove that out of all the morphological parameters, these groups of parameters exhibit the strongest correlation with the solar potential indicators and were effective preliminary evaluation indicators of solar performance of the high-density residential

areas. Furthermore, given that SS_{U600} and SS_{U400} became easily obtainable through quick calculations without relying on the simulation software, they automatically became useful as effective predictive parameters in the early design stage.

These findings are informative to urban planners and architects, and they also suggest that increasing the value of SS_{U600} and SS_{U400} is an effective way to raise the solar potential during the planning and design process. To be more specific, the following methods were proven to be effective in Section 4.1:

(a). Lowering the building height and increasing the number of buildings to augment the roof area;
(b). Adjusting the building to the suitable orientation which is conducive to raising the value of SSU600 and SSU400;
(c). Or adjusting the building plan shape to make more facades be beneficial for solar receiving.

5.2. Effectiveness of the Prediction Model

On the basis of the correlation analysis, the mathematical relationships between several morphological parameters and the solar potential indicators were established via a multiple linear regression analysis, namely the prediction model. The purpose of building predictive models was to calculate solar potential quickly by using the morphological parameters variables exclusively as model inputs, which might enable designers and decision makers to evaluate or compare the solar performance of the respective schemes in the early design stage.

The verification results of the aforementioned five cases are revealed in Figures 10 and 11. It can be concluded that the predicted values of four cases coincide with the simulation values, while the predictive range of case 04 deviated from the simulation value. The master plan of case 04 clearly depicts that the site's east side was vacant with no building obstruction, which made it more favorable for solar energy reception. This explains why the simulation value was higher than the predicted values. For subsequent calculation purposes, the assumption that the site was surrounded by the plots with same layout was made.

In summary, this exercise showcases how the solar indicators SR_{U600} and SR_{U400} can be calculated quickly using morphological parameters as the model input in an early design stage. It is also demonstrated that the prediction models (2) and (3) were probably workable in boundary condition.

6. Conclusions and Limitations

6.1. Conclusions

This paper takes Shanghai as an example to study the relationship between the morphological parameters and the solar potential performance indicators of high-density residential areas. A total of 1260 parametric scenarios and five real cases were selected respectively for exploratory research and case verification through a customized workflow. Two solar performance indicators SR_{U600} and SR_{U400} were calculated corresponding to the thresholds 600 kWh/m^2/y and 400 kWh/m^2/y respectively. In addition to the well-known morphological parameters, two new parameters SS_{U600} and SS_{U400} were proposed since their abilities to depict the properties of solar irradiation receiving of the building envelope surfaces were validated. The results showed that there were strong linear correlations between SS_{U600}/SS_{U400} and SR_{U600}/SR_{U400}, and the correlation coefficients R^2 reached 0.874 and 0.933 respectively. This finding suggests that SS_{U600} and SS_{U400} are effective preliminary evaluation indication parameters of solar performance in high density residential areas. The morphology optimization methods—such as reducing the building height and increasing the number of buildings, adjusting the building to a suitable orientation, adjusting the building plan shape, etc.—were able to increase both SR_{U600} and SR_{U400} effectively.

The prediction models of solar performance indicators were established with morphological parameters as independent variables. In the boundary condition, their validity of was verified through comprehensive analysis of real cases.

The research methodology developed in this study can serve as reference for related performance-based urban design and planning and is also applicable to other geographic regions and building types. The findings offer a solid foundation for quantitative understanding of the correlation between the city's morphology and solar potential and provide hints for morphological optimization designs based on solar energy utilization.

6.2. Limitations and Future Studies

In this study, the findings were based on limited number of typical residential scenarios and cases, hence should be interpreted with caution. More typologies and cases with complex surroundings, non-homogeneous building heights and construction details (balcony, roof form, etc.) shall be examined in the future. The simulation of solar irradiation was conducted using Shanghai's weather data and the generalizability of the findings should be examined in the other cities. Moreover, the simulated results shall be verified against measured data to further ascertain the findings and conclusions. The current study essentially focuses on solar energy potential. In order to come up with a more comprehensive understanding of solar energy utilization, future research could take into consideration the various ways of using solar energy—such as daylight, PV, and ST—and their associated effectiveness. Another emphasis for future works is the integrated performance evaluation of buildings—such as daylight availability, heat insulation, and so on—which may affect each other, hence, their interactions should be researched systematically.

References

1. Bank, W. Cities and Climate Change: An Urgent Agenda. 2010. Available online: openknowledge.worldbank.org (accessed on 9 January 2018).
2. Freitas, S.; Catita, C.; Redweik, P.; Brito, M.C. Modelling solar potential in the urban environment: State-of-the-art review. *Renew. Sustain. Energy Rev.* **2015**, *41*, 915–931. [CrossRef]
3. Sarralde, J.J.; Quinn, D.; Wiesmann, D. Urban modelling for resource performance analysis: Estimating cities' renewable energy potential. In Proceedings of the Building Simulation, Sydney, Australia, 14–16 November 2011; pp. 1370–1377.
4. China National Energy Administration. *The 13th Five-Year Plan for Energy Development*; China National Energy Administration: Beijing, China, 2016.
5. Ronneberger, O.; Fischer, P.; Brox, T. U-Net: Convolutional Networks for Biomedical Image Segmentation. In Proceedings of the 18th International Conference on Medical Image Computing and Computer Assisted Intervention, Munich, Germany, 5–9 October 2015.
6. *Regulations of Shanghai Municipality on Building Energy Conservation*; Shanghai Municipal People's Congress: Shanghai, China, 2010.
7. Heng, C.K.; Malone-Lee, L.C.; Zhang, J. Relationship between density, urban form and environmental performance. In *Growing Compact: Urban Form, Density and Sustainability*; Bay, J.H., Lehmann, S., Eds.; Routledge: London, UK, 2017.
8. Okeil, A. In Search for Energy Efficient Urban Forms: The Residential Solar Block. In *Building for the Future: The 16th CIB World Building Congress 2004*; In-House Publishing: Rotterdam, The Netherlands, 2004.
9. Leung, K.S.; Steemers, K. Exploring solar-responsive morphology for high-density housing in the tropics. In Proceedings of the CISBAT 2009, Lausanne, Switzerland, 2–3 September 2009.

10. Kanters, J.; Wall, M. The impact of urban design decisions on net zero energy solar buildings in Sweden. *Urban Plan. Transp. Res.* **2014**, *2*, 312–332. [CrossRef]

11. Kanters, J.; Wall, M.; Dubois, M.-C. Development of a Façade Assessment and Design Tool for Solar Energy (FASSADES). *Buildings* **2014**, *4*, 43–59. [CrossRef]

12. Available online: www.solarplanning.org (accessed on 5 January 2017).

13. Dapeng, L.; Gang, L.; Shengming, L. Solar potential in urban residential buildings. *Solar Energy* **2015**, *111*, 225–235.

14. Mohajeri, N.; Upadhyay, G.; Gudmundsson, A.; Assouline, D.; Kämpf, J.; Scartezzini, J.-L. Effects of urban compactness on solar energy potential. *Renew. Energy* **2016**, *93*, 469–482. [CrossRef]

15. Caroline, H.; Andreas, A.; Paul, F. Evaluation of energy supply and demand in solar neighborhood. *Energy Build.* **2012**, *49*, 335–347.

16. Peronato, G.; Nault, E.; Cappelletti, F. A parametric design-based methodology to visualize building performance at the neighborhood scale. In Proceedings of the Building Simulation Applications 2015, Bolzano, Italy, 4–6 February 2015.

17. Chatzipoulka, C.; Compagnon, R.; Kämpf, J.; Nikolopoulou, M. Sky view factor as predictor of solar availability on building façades. *Solar Energy* **2018**, *170*, 1026–1038. [CrossRef]

18. Ji, Z.; Le, X.; Veronika, S.; Stephen, E.T.; Huixuan, S.; Stephen, S.L.; Thomas, R. Impact of urban block typology on building solar potential and energy use efficiency in tropical high-density city. *Appl. Energy* **2019**, *240*, 513–533.

19. Montavon, M.; Scartezzini, J.L.; Compagnon, R. Comparison of the solar energy utilization potential of different urban environments. In Proceedings of the Plea 2004 Proceedings of 21st Conference on Passive and Low Energy Architecture, Eindhoven, The Netherlands, 19–21 September 2004; pp. 1733–1748.

20. Cheng, V.; Steemers, K.; Montavon, M.; Compagnon, R. Urban Form, Density and Solar Potential. In Proceedings of the PLEA 2006—23rd International Conference on Passive and Low Energy Architecture, Geneva, Switzerland, 6–8 September 2006.

21. Yijia, D. Urban Morphology Study and Explanation on Prototype of Contemporary Condominium in Shanghai. Ph.D. Thesis, Tongji University, Shanghai, China, 2015.

22. Huang, Z.; Shen, G. *Shanghai Excellent Residential Design 2000*; China Building Industry Press: Beijing, China, 2001.

23. Huang, Z.; Shen, G. *Shanghai Excellent Residential Design 2002*; China Building Industry Press: Beijing, China, 2003.

24. Huang, Z.; Shen, G. *Shanghai Excellent Residential Design 2004*; China Building Industry Press: Beijing, China, 2005.

25. Huang, Z.; Shen, G. *Shanghai Excellent Residential Design 2006*; China Building Industry Press: Beijing, China, 2007.

26. Huang, Z.; Shen, G. *Shanghai Excellent Residential Design 2008*; China Building Industry Press: Beijing, China, 2009.

27. Huang, Z.; Shen, G. *Shanghai Excellent Residential Design 2010*; Shanghai Survey and Design Industry Association Press: Shanghai, China, 2011.

28. *Design Standard for Residential Buildings*; DGJ08-20-2013; Shanghai Urban Construction and Communications Commission: Shanghai, China, 2013.

29. Compagnon, R. Solar and daylight availability in the urban fabric. *Energy Build.* **2004**, *36*, 321–328. [CrossRef]

30. Berghauser Pont, M.; Haupt, P. Space, Density and Urban Form. Ph.D. Thesis, Delft University of Technology, Delft, The Netherlands, 2009.

31. Weather Data for Ladybug. Available online: https://energyplus.net/weather-search/shanghai (accessed on 2 May 2018).